Mechanical State of Gravel Soil in Mobilization of Rainfall-Induced Landslide in Wenchuan seismic area, Sichuan province, China

Liping Liao[1,2,3], Yunchuan Yang[1,2,3], Zhiquan Yang[4], Yingyan Zhu[5*] , Jin Hu [5], D.H.Steve Zou[6]

[1]College of Civil Engineering and Architecture, Guangxi University, Nanning 530004, China

[2]Key Laboratory of Disaster Prevention and Structural Safety of Ministry of Education, Guangxi University, Nanning 530004, China

[3]Guangxi Key Laboratory of Disaster Prevention and Engineering Safety, Guangxi University, Nanning 530004, China

[4]Faculty of Land Resource Engineering, Kunming University of Science and Technology, Kunming 650500, China

[5]Institute of Mountain Hazards and Environment, Chinese Academy of Sciences and Ministry of Water Conservancy, Chengdu 610041, China

[6]Department of Civil and Resource Engineering, Dalhousie University, Halifax, NS, Canada B3H4K5

Correspondence to: Y. Y. Zhu (zh_y_y_imde@163.com)

Abstract Gravel soils generated by Wenchuan earthquake have undergone natural consolidation for the past decade. However, geological hazards, such as slope failures with ensuing landslides, have continued to pose the great threats to the region. In this paper, artificial model tests were used to observe the changes of soil moisture content and pore water pressure, as well as macroscopic and microscopic phenomena of gravel soil. In addition, the mathematical formula of the critical state was derived from the triaxial test data. Finally, the mechanical states of gravel soil were determined. The results had five aspects. (1) The time and mode of the occurrence of landslide were closely related to the initial dry density. The process of initiation was accompanied by changes in density and void ratio. (2) The migration of fine particle and the rearrangement of coarse-fine particle contributed to the reorganization of the microscopic structure, which might be the main reason for the variation of dry density and void ratio. (3) If the confining pressure was same, the void ratios of soils with constant particle composition would approach to approximate critical values. (4) Mechanical state of gravel soil can be determined by the relative position between state parameter (e, p') and e_c-p' planar critical state line, where e was the void ratio, e_c was the critical void ratio and p' was the mean effective stress. (5) In the process of landslide initiation, dilatation and contraction were two types of gravel soil state, but dilatation was dominant. This paper provided an insight to interpret landslide initiation from the perspective of critical state soil mechanics.

Keywords Mechanical state • gravel soil• landslide• critical state• Wenchuan seismic area

1   Introduction

In 2008, the gravel soil generated by Wenchuan earthquake produced a large amount of loose deposits (Tang and Liang 2008; Xie et al., 2009). These deposits had features such as wide grading, weak consolidation and low density. They were located on both sides of roads and gullies, and led to the formation of soil slopes (Cui et al., 2010; Qu et al., 2012; Zhu et al., 2011). Although gravel soils have subjected to natural consolidation process for nearly a decade, geological hazards, such as slope failures with ensuing landslides, are readily to motivate in rainy season. At present, geo-hazards still pose the great threats to the region (Chen et al., 2017; Cui et al., 2013; Yin et al., 2016).

The variation of mechanical state, such as the transformation from a relatively stable state to a critical state, has been commonly used to analyze the initiation of landslides (Iverson et al., 2010; Iverson et al., 2000; Liang et al., 2017; Sassa 1984; Schulz et al., 2009). Therefore, a deep understanding of the soil state is the scientific basis for the study of landslide occurrence (Chen et al., 2017). Generally, the critical void ratio is an important parameter to determine the state of soil quantitatively (Been and Jefferies 1985; Schofield and Wroth 1968). The theoretical research had its origins in Reynold's work in 1885. He defined the characteristic of the volumetric deformation of granular materials due to shear strain as dilatation (Reynolds 1885). Casagrande (1936) pointed out that loose soil contracted, and dense soil dilated to the same critical void ratio in the drained shearing test. He drew the F line to distinguish the dilative zone and the contractive zone. The F line's horizontal and vertical coordinate is effective normal stress and void ratio. Since the 1980s, critical state soil mechanics received extensive attentions (Fleming et al., 1989; Gabet and Mudd 2006; Iverson et al., 2000). Some of the observed landslides, such as the Salmon Creek landslide in Marin County (Fleming et al., 1989), Slumgullion landslide in Colorado (Schulz et al., 2009), and Guangming New Distinct landslide in Shenzhen (Liang et al., 2017), might be approximately explained by this theroy. Based on the F line drawn by Casagrande (1936), Fleming (1989) found that the increase of pore water pressure contributed to the dilation, and causes the debris flow characterized by the intermittent movement. Iverson (1997; 2000)pointed out porosity played an important role in the occurrence of landslide; in the soil shearing process, the density of loose sand increased, and the density of dense sand decreased to the same critical density. The formula of the void ratio was derived, which was the function of the mean effective stress (Gabet and Mudd 2006). William et al (2009) found out the dilative strengthening might control the velocity of a moving landslide through the hourly continuous measurement of displacement of landslide. Liang et al (2017) found that the initial solid volume fraction affect the soil state of the granular-fluid mixture. Other scholars also found that in the shearing process, dilation or contraction was exiting in residual soil, loess and coarse-grained soil (Dai et al., 2000; Dai et al., 1999a; Dai et al., 1999b; Liu et al., 2012; Zhang et al., 2010).

The above researchers provided the meaningful insights to explain the occurrence of landslides and drawn the instructive conclusion, such as the initial density or porosity can affect the mechanical state of soil (Iverson et al., 2000) and the formation of landslide (McKenna et al., 2011). However, most of them focused on qualitative results and lacked mutual verification between indoor test and model test. In addition, for the gravel soil generated by seismic, the study on its mechanical state is lacking. Some scientific issues need to be solved. For example, what are the differences and similarities of landslide occurrence? Why does the void ratio or the density change? Is the mechanical state, a contraction or dilation? The purpose of this paper is to solve the above issues through artificial flume model tests and triaxial tests. Firstly, the macroscopic phenomena were

observed and summarized. Secondly, the variations of soil moisture content and pore water pressure were analyzed. Thirdly, the microscopic property of soil was obtained. Fourthly, the mathematical expression of critical state of soil was proposed. Finally, the mechanical state of gravel soil was determined by the relative position between state parameter (e, p') and e_c-p' planar critical state line.

2   Field site and method

2.1   Field site

Niujuan Valley is located in Yingxiu town of Wenchuan County, Sichuan Province, which is the epicenter of 12 May 2008 Wenchuan earthquake in China (Fig.1). The main valley of the basin has an area of 10.46km^2, and a length of 5.8km. The highest elevation is 2693m, and the largest relative elevation is 1833m. The gradient ratio of the valley bed is 32.7%~52.5% (Tang and Liang 2008; Xie et al., 2009). Six small ditches are distributed in the basin. Most of the valley is covered with the abundant gravel soil. Extreme complicate terrain and adequate rainfall triggers the frequent landslides and the large-scale debris flows. Thus, this valley is the most typical basin in the seismic area. Its excellent landslide formative environment can provide comprehensive reference models and abundant soil samples for artificial flume model tests.
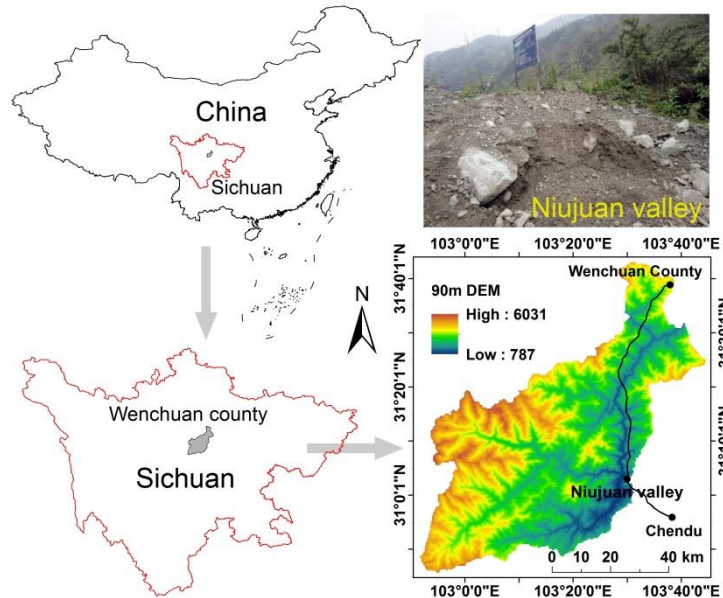
Fig. 1 Study area

2.2   Soil tests and quantitative analysis

2.2.1   Artificial flume model test

Based on the field surveys along Duwen highway, Niujuan valley and the literature review (Chen et al., 2010; Fang et al., 2012; Tang et al., 2011; YU et al., 2010), most of the rainfall induced landslides is shallow. The range of the slope angle is 25°~40° and its average value is 27°. The rainfall intensity triggering the landslide is 10mm/h~70mm/h. As shown in Fig.2(a). The length, width and height of the flume model are 300cm, 100cm and 100cm.

The gravel soil samples are from Niujuan valley. The specific gravity is 2.69. The range of dry density is 1.48~2.36g/cm^3; in addition, the minimum and the maximum void ratio is 0.14 and 0.82. Fig.2(b) shows that the cumulative content of gravel (diameter<2mm) and silt and clay (diameter<0.075mm) is 30.74% and 2.78%. The content of silt and clay plays the important role in

the mobilization of landslide and debris flow (Chen et al., 2010). Four initial dry densities are designed as 1.50g/cm³,1.60g/cm³, 1.70g/cm³ and 1.80g/cm³. According to the previous investigations, the water content mainly changes within a depth less than 50cm, and its average value varies from 6%~8%, while water content below 50cm basically keeps stable. Therefore, the total thickness of the soil model is 60cm. In order to achieve a predetermined initial dry density, the soils of the models are divided into four layers, and each layer is compacted respectively. The thickness of each layer is 20cm, 15cm, 15cm and 10cm (Fig.2(a)). Due to the experiment error, the actual initial dry density (IDD) is 1.54g/cm³, 1.63g/cm³, 1.72g/cm³ and 1.81g/cm³ (Tab.1).

Artificial rainfall system, designed by the Institute of Soil and Water Conservation, Chinese Academy Science, comprises of two spray nozzles, a submersible pump, water box and a bracket. The range of nozzle sizes is 5~12mm, thus, the different rainfall intensity can be simulated. The rain intensity triggering the large-scale debris flow on 21, August, 2011 is 56.5mm/h, which is the designed rainfall for test. The real rainfall intensity is 47~50.2mm/h because the model test is disturbed by the direction of wind. Three groups of sensors, including the micro-pore pressure sensors (the model is TS-HM91) and moisture sensors (the model is SM300), are placed between two layers of the soil to measure the volume water content and the pore water pressure (Fig.2(a)). A data-acquisition system (the model is DL2e) is used to collect the data; it can scan 30 channels within the same second. A camera is used to record the macroscopic process of the entire experiment.

2.2.2 Triaxial test

Tests are performed by using a dynamic apparatus in Institute of Mountain Hazards and Environment, Chinese Academy Science. The diameter and the height of sample are 15 cm and 30 cm (Fig.3). Test is the saturated and consolidated drainage shear test at a shear rate of 0.8mm/minute, which comprises of two sets: the initial dry density of 1.94 and 2.00g/cm³. The confining pressure σ_3 is 50Kpa, 100Kpa and 150Kpa.
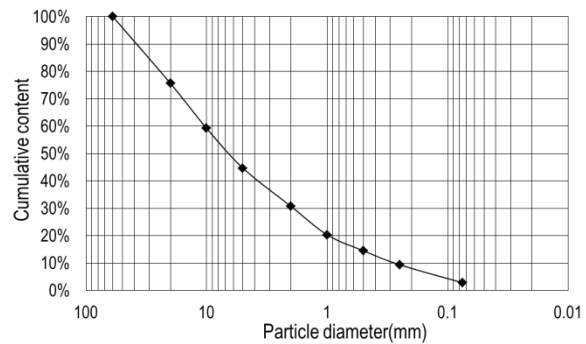
(a) Artificial flume model (the position of sampling: red line-1#, pink line-2#, white line-3#)   (b) Grain composition of gravel soil

Fig. 2 Test model and grain composition of gravel soil

Tab. 1 Sets of artificial flume model test

Factor Number	Initial volume moisture content (%)	Slope angle(°)	Rainfall intensity (mm/h)	Initial dry density (g/cm³)
1				1.54
2	6~8	27	47~50.2	1.63
3				1.72
4				1.81

Fig. 3 Dynamic triaxial apparatus

2.2.3 Quantitative analysis method

Quantitative analysis is mainly based on artificial flume model test and triaxial test. Firstly, the state parameters of soil are represented by the void ratio e and the mean effective stress p', which are from the model test. In model test, at least three soil samples are collected by soil sampler in the same depth of the line 1#, 2# and 3#, and are used to calculate their natural density ρ, mass moisture content ω and dry density ρ_d. Later, e can be calculated by the formula: $e=G_s/\rho_d-1$ (G_s is the specific gravity). The cumulative content of coarse P_5 (particle diameter > 5mm), gravel (particle diameter < 2mm) P_2, and silt and clay (particle diameter < 0.075mm) $P_{0.075}$ is obtained from the particle grading tests. p' can be calculated by the formula: $p'=(\sigma_x+\sigma_y+\sigma_z)/3$, where $\sigma_z=\gamma h$ and $\sigma_x=\sigma_y=K_a\gamma h$. h is the vertical distance between a certain point inside the slope and the surface of the slope; β is the slope angle. γ is the unit weight of soil. K_a is the lateral pressure coefficient, which can be calculated by the formula (1) (Chen et al., 2012). ϕ is the internal friction angle of soil. In this paper, $\beta=27°$, $\phi=33°$.

$$K_a = \cos\beta \frac{\cos\beta - \sqrt{\cos^2\beta - \cos^2\phi}}{\cos\beta + \sqrt{\cos^2\beta - \cos^2\phi}} \tag{1}$$

Secondly, the critical state line (CSL) is derived from the triaxial test. Finally, based on the critical state soil mechanics, according to the relative position of the state parameter (e, p') at the CSL, the mechanical state of the soil can be estimated. When the soil state (e, p') is located at the upper right of the CSL, the soil is contracted. When the soil state (e, p') is located at the lower left of the CSL, the soil is dilated (Casagrande A 1936; Schofield and Wroth 1968).

3 Results

3.1 Macroscopic phenomena of experiment

According to the record by a camera, when IDD is 1.54~1.72g/cm³ except 1.81g/cm³, the landslide can be triggered by rainfall. The processes of the occurrences of landslides have their similarity and difference. The similarity is that at the beginning of rainfall, the shallow soil is compacted by seepage force and soil weight (Fig.4(a)). In addition, during the rainfall duration, surface runoff cannot be observed, whereas muddy water appears and overflows the slope foot (Fig. 4(b)). This phenomenon indicates that the entire rainfall can seep into the internal soil, followed by the formation of subsurface flow. At this moment, the fine particles along the percolation paths begin to move in translation and rotation under the action of gravity (Gao et al., 2011; Igwe 2014) and cause a re-distribution of the microstructure of soil (Chen et al., 2004; Zhuang et al., 2015). These moving fine particles will fill the interval space of porosity, even block the downstream channels of the seepage path (Fang et al., 2012; McKenna et al., 2011), which can lead to a decrease in void ratio and an increase of the pore water pressure (Gao et al., 2011).

The difference of experiment is time and mode of the occurrence of landslide. When IDD is 1.54~1.63g/cm^3, the total time of landslide occurrence is 30~40 minutes, including the time of partial sliding and overall sliding. The processes of landslide occurrence involve three steps. Firstly, the partial soil of the superficial layer slowly slides in the shape of mudflow when rainfall duration is about 8min (Fig. 5(a)). Secondly, small-scale slips occur in a layered manner (Fig. 5(b)). Thirdly, the overall sliding is motivated when the rainfall duration is about 33min (Fig. 5(c)). The above processes represent the mode of landslide is the progressive failure. This mode reflects four mechanisms. Firstly, in the early stage of rainfall, the shearing strength of shallow soil decreases and partial sliding appears due to the rapid infiltration of rainfall. Secondly, partial sliding takes away the saturated soil, which causes the internal soil exposed on the surface. Thirdly, the exposed soil slides again, which can change the geometrical shape of the slope and prompt the shearing force increase. Fourthly, when the increase of the shearing force can destroy the balance of the slope, overall sliding will appear.

When IDD is 1.72g/cm^3, the total time of landslide occurrence is 18 minutes. Landslide formation process is divided into three steps. Firstly, the shear opening gradually occurs accompanied by the visible cracks developing in the slope foot (Fig. 6(a)). Secondly, surface cracks begin to develop on the slope top (Fig. 6(b)). Finally, landslide initiates accompanied by the instantaneous propagation of cracks (Fig. 6(c)~(d)), which takes 5s. The above steps imply the mode of landslide is the tractive failure. The mechanism includes three aspects. Firstly, an increase in soil weight causes an increase in shearing force, which breaks the equilibrium state of slope, so cracks can develop in the slope foot and cause the shear opening. Secondly, the instability of the slope continues to deteriorate, which leads to new cracks located at the top of the slope. Thirdly, the overall sliding is triggered by crack extension.

When IDD is 1.81g/cm^3, the shearing opening appears at the slope foot (Fig. 7(a)). In the next, the muddy water can flow from the slope foot (Fig. 7(b)). Even though on the slope surface, fine particles disappear and coarse particles are exposed, rainfall could not trigger a landslide (Fig. 7(c)). One reason is that the fine particles within the surface soil move with the water seepage. After the fine particles of the shallow soil are all migrated, the soil skeleton begins to consist of coarse particles. This skeleton can provide some smooth paths for the subsurface runoff. The other reason is that when the soil is in a dense state, the change of volume moisture content is limited due to the low permeability. Even if the soil shows a small shearing strain, the loss of pore water pressure is difficult to recover in time due to the lack of rainfall infiltration. Therefore, the shearing strength can remain unchanged.

Macroscopic phenomena of experiments imply that the initial dry density can influence the time and mode of landslide occurrence. It coincides with the existing research (Iverson et al., 2000). As the IDD increases from 1.54g/cm^3 to 1.72g/cm^3, the failure mode of soil changes from progressive sliding to traction sliding. When IDD is less than 1.63g/cm^3, partial sliding is a dominant phenomenon that affects the entire deformation failure. When IDD is 1.72g/cm^3, shear opening and cracks are responsible for deformation failure. Although the total time of overall sliding of loose soil is longer than that of relatively dense soil, the time of partial sliding is shorter. This difference may be associated with failure modes, and relative time scales of shearing strength loss and changes of pore water pressure.

208
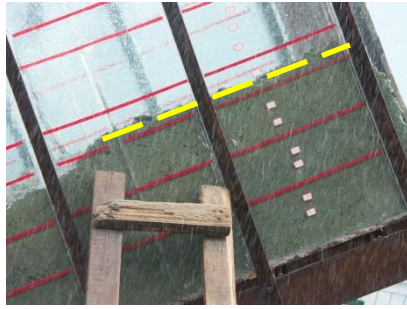
(a) Shallow soil is compacted   **(b) Muddy water is generated**

209   **Fig. 4 Similarity of process of landslide initiation**

210

(a) Soil of the superficial layer slowly slides   **(b) A small-scale slip occurs**

212
213

(c) The overall slide is motivated

214   **Fig. 5 Process of landslide initiation (IDD of 1.54~1.63g/cm^3)**

215
216

(a) Shearing opening appears in slope foot   **(b) Cracks develop on the slope top**

217
218

(c) Crack propagation   **(d) Landslide is triggered**

219   **Fig. 6 Process of landslide initiation (IDD of 1.72g/cm^3)**

(a) Shearing opening appears at the slope foot   **(b) Muddy water flows from the slope foot**

(c) Fine particles disappears and coarse particles are exposed

Fig. 7 Process of experiment (IDD of 1.81g/cm^3)

3.2 Volume moisture content (VMC) and pore water pressure (PWP)

The maximum x label in Fig.8 ~ Fig.10 represents the total time for the occurrence of the landslide. This value is also the rainfall duration. In order to compare with Fig.8 ~ Fig.10, the maximum x label in Fig.11 is 1800s. As shown in Fig.8 to Fig.11, the first change is VMC of the depth of 10cm, followed by VMC of the depth of 25cm and 40cm. This change order of VMC is related to the process of rainfall penetration. Especially, rainfall penetration is from shallow soil to deep soil. Therefore, the VMC of 10cm can increase first. The variation of VMC at the depth of 10~25cm exhibits a similar tendency. The tendency consists of three phases. Since the beginning of rainfall, VMC has been in a constant state. When the rainfall seeps into soil, VMC increases rapidly and eventually grows steadily. The time when VMC of the depth of 10cm begins to increase is 203s, 292s, 313s for 1.54~1.72g/cm^3. This result indicates these three densities have different permeability, the higher density, the lower hydraulic conductivity and the longer time of penetration. The time when VMC of the depth of 25cm begins to increase is about 900s for 1.54~1.72g/cm^3.

When IDD is 1.54g/cm^3 and 1.63g/cm^3, VMC at a depth of 40cm initially remains stable and eventually shows an increasing trend. Change trend of 1.54g/cm^3 is more obvious than that of 1.63g/cm^3. When IDD is 1.72g/cm^3, VMC at a depth of 40cm is almost constant. The reason is that when a landslide occurs, rain stops; at this time, no abundant water can penetrate to this depth. When IDD is 1.81g/cm^3, if the rainfall duration is less than 1300 seconds, VMC of 40cm remains stable. When the duration is about 1300 seconds, compared to Fig.8 to Fig.10, VMC of 40 cm starts to increase. This difference between Fig.11 and other three figures may be attributed to the following aspect. As mentioned in section 3.1, the landslide cannot be triggered by rainfall. Therefore, there is sufficient time for rainfall to penetrate to a depth of 40cm, although the hydraulic conductivity is low. However, when the rainfall time is greater than 1800 seconds, VMC of 10~40cm keeps constant. This means due to the accumulation of fine particle, there may be an impermeable layer in the depth of 0~10cm. This layer can prevent rain penetrate deeper than 10cm. When rainfall continues, rainfall can be converted into the subsurface runoff, flowing out of the soil skeleton that consists of coarse particles.

As shown in Fig.8 to Fig.11, PWP at a depth of 10~25cm has a similar tendency. This tendency consists of a sharp increase at first, a rapid decrease and a continuous dynamic fluctuation. However, the variation of PWP is inconsistent with the variation of VMC. Before VMC increases, PWP with the depth of 10cm~25cm has experienced the sharp increase and decrease. Soil inhomogeneity may contribute to this inconsistence. As mentioned in 3.1, at the beginning of experiment, the surface layer less than 10cm is compacted by seepage force and soil weight. The compaction and penetration process leads to the increase of the force acting on the subsoil, which causes the increase of PWP. During the saturation process of the surface layer, the fine particles of this layer are taken away and fill the porosity of the subsoil, which prompt PWP to the peak value quickly. When the surface soil slowly moves or cracks begin to develop in the slope foot, the internal deformation due to dilation will occur, which causes PWP releases. When VMC increases, PWP has a dynamic fluctuation. This fluctuation may be attributed to the rearrangement of the soil skeleton.

The curve of PWP with a depth of 40cm is drawn above that of 10~25cm. The variation has no significant increase or decrease, but exhibits a smooth fluctuation. During the whole rainfall duration, the corresponding VMC shows that the soil is not saturated. Therefore, the pore pressure of 40cm is dominated by air pressure.
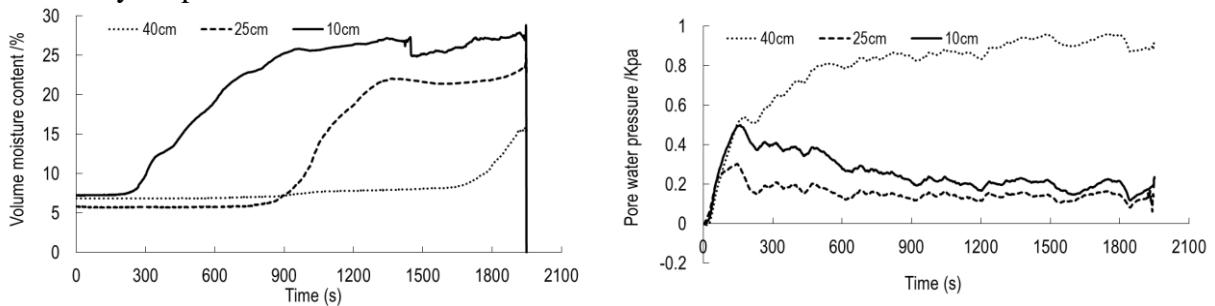
Fig. 8 Volume moisture content and pore water pressure when IDD is 1.54g/cm^3
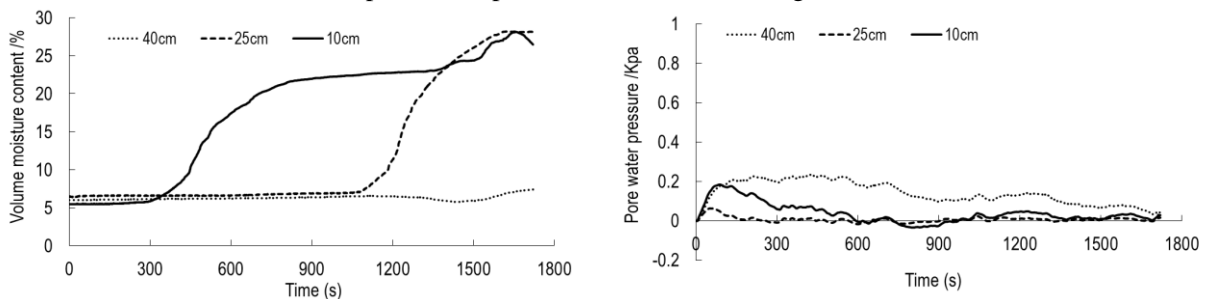
Fig. 9 Volume moisture content and pore water pressure when IDD is 1.63g/cm^3
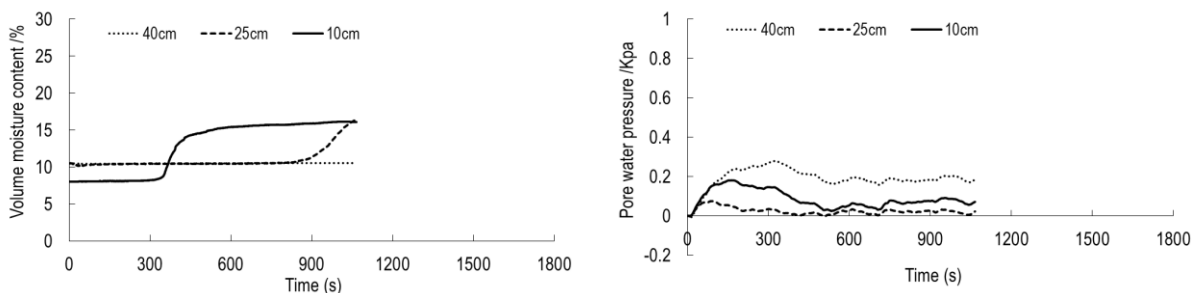
Fig. 10 Volume moisture content and pore water pressure when IDD is 1.72g/cm^3
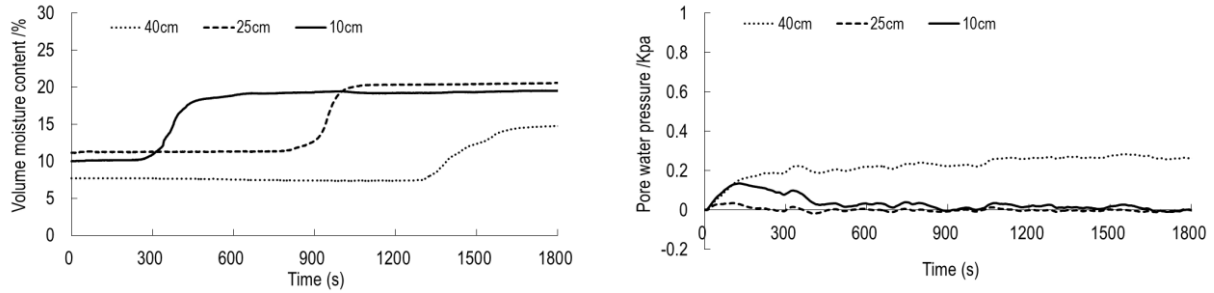
274
275 **Fig. 11** Volume moisture content and pore water pressure when IDD is 1.81g/cm³

3.3 Microscopic property of gravel soil

277   As shown in Tab.2, when IDD is from 1.54 to 1.72g/cm³, the natural density and the dry density
278 with the depth of 5cm~20cm are larger than those before the tests, and the void ratio is less than that
279 before the tests. Of these three lines, the line 1# has the greatest change rate in density. When IDD is
280 1.63cm³, the density of 40cm is less than the value before the test. When IDD is 1.81g/cm³, the
281 densities with the depth of 5~10cm are increased compared to that before the test.

282 **Tab 2.** Density and void ratio of gravel soil with initial dry density 1.54~1.81g/cm³

Number	Initial dry density (g/cm³)	Line number	Soil depth h (cm)	Natural density ρ (g/cm³)	Mass moisture content ω (%)	Dry density ρ_d (g/cm³)	Void ratio $e=G_s/\rho_d-1$	$\sigma_z=\gamma h$ (Kpa)	$\sigma_x=\sigma_y=K_a\gamma h$ (Kpa)	$p'=(\sigma_x+\sigma_y+\sigma_z)/3$ (Kpa)
1	1.54	3#	5	2.08±0.05	9.35±0.85	1.90±0.04	0.39±0.03	1.04	0.59	0.74
		3#	28	1.93±0.03	8.61±1.16	1.77±0.02	0.49±0.02	5.39	3.07	3.84
		2#	33	2.07±0.05	9.15±0.15	1.89±0.04	0.40±0.03	6.82	3.88	4.86
		1#	21	2.10±0.05	9.63±1.01	1.91±0.05	0.39±0.04	4.40	2.51	3.14
2	1.63	3#	5	2.19±0.01	13.36±0.09	1.98±0.01	0.34±0.01	0.44	0.25	0.31
		3#	40	1.67±0.03	6.15±0.17	1.58±0.02	0.68±0.02	6.68	3.80	4.76
		2#	20	2.09±0.04	10.18±0.21	1.90±0.04	0.39±0.03	4.19	2.38	2.99
		1#	13	2.23±0.04	10.84±0.83	2.01±0.02	0.32±0.02	2.90	1.65	2.07
3	1.72	3#	10	2.22±0.02	8.45±0.72	2.05±0.02	0.30±0.01	2.22	1.26	1.58
		3#	25	2.34±0.04	8.59±0.261	2.16±0.05	0.23±0.03	5.86	3.33	4.17
		1#	10	2.30±0.01	9.26±0.42	2.10±0.01	0.26±0.01	2.30	1.31	1.64
4	1.81	3#	5	2.14±0.04	9.57±0.75	1.95±0.04	0.36±0.03	1.28	0.73	0.91
		3#	10	2.26±0.01	8.16±0.39	2.09±0.02	0.27±0.01	2.26	1.28	1.61

283   As shown on section 2.2.1, P_5 before the test is 55.32%. Therefore, coarse particles and fine
284 particles interact to form the soil skeleton, which affects changes in dry density (Guo 1998) and
285 landslide characteristics (Li et al., 2014). In this paper, the particle content before and after the test is
286 compared to understand the change in the void ratio. As shown in Tab.3, when IDD is 1.54g/cm³ and
287 1.63g/cm³, the loss of $P_{0.075}$ of the shallow soil of line 3# is the largest, followed by that of line 1#.
288 The result indicates that the fine particles of surface soil at the slope top begin to move along
289 direction of gravity firstly. When subsurface runoff forms, these particles begin to move to the slope
290 foot. This process causes two results. One is that the porosity of the position related to particle
291 migration increases. The other is that the porosity filled by fine particles decreases (Fang et al., 2012;
292 McKenna et al., 2011), which is the seepage-compacting effect (Jiang et al., 2013). As a result, the
293 shallow soil of the slope top is looser than that of the slope foot. The loss of $P_{0.075}$ ($\triangle P_{0.075}$, which is
294 negative) at the slope top decreases significantly with depth. Especially, it is about -1.26% at the
295 depth of 40cm. It implies that the depth of rainfall infiltration is about 40 cm. In the case of IDD of
296 1.72g/cm³~1.81g/cm³, the variation of $P_{0.075}$ of the slope top changes from negative to positive

297 accompanied by the increase of depth. This trend indicates that the fine particles may concentrate at
298 the depth of 5~25cm. The depth range of particle concentration is 10~25cm, 5~10cm for 1.72g/cm^3
299 and 1.81g/cm^3.

300 **Tab 3.** Variation of coarse and fine particles contents

Number	Initial dry density (g/cm^3)	Line number	Soil depth$h$ (cm)	P_5	$\triangle P_5$	$P_{0.075}$	$\triangle P_{0.075}$	P_2	$\triangle P_2$
1	1.54	3#	5	61.00%	10.25%	0.66%	-76.24%	30.69%	-0.16%
		3#	28	55.91%	1.05%	2.01%	-27.90%	34.36%	11.76%
		1#	21	58.98%	6.60%	0.77%	-72.36%	31.07%	1.05%
2	1.63	3#	5	58.69%	6.09%	0.91%	-67.23%	31.40%	2.15%
		3#	40	57.98%	4.80%	2.75%	-1.26%	31.69%	3.07%
		1#	13	67.66%	22.30%	1.26%	-54.81%	26.23%	-14.68%
3	1.72	3#	5	55.98%	1.18%	1.03%	-62.98%	32.70%	6.38%
		3#	10	54.01%	2.37%	1.78%	-36.14%	33.94%	10.40%
		3#	25	55.32%	0%	3.17%	13.85%	34.05%	10.75%
		1#	10	56.15%	1.5%	1.42%	-49.09%	33.67%	9.53%
4	1.81	3#	5	52.50%	-5.11%	2.06%	-25.83%	35.49%	15.45%
		3#	10	52.55%	-5.01%	2.86%	2.68%	33.91%	10.30%

301 Note: the positive value of the change represents an increase while the negative value represents a decrease.

302 On the slope top, P_5 at a depth of 5cm changes from positive to negative with the increasing of
303 IDD, which range is from -5.11% to 10.25%. The reason is that the loss of fine particles contributes
304 to the relatively increase of the content of coarse particles. Both $P_{0.075}$ on the slope top and $P_{0.075}$ on
305 the slope foot decreases. The range of $\triangle P_{0.075}$ is from -25.83% to -76.24% and from -49.09% to
306 -72.36% accordingly. The relationship between $\triangle P_{0.075}$ and ρ_d is shown in Fig.12. The regression
307 equation is as follows: $\triangle P_{0.075}=1.2632\rho_d - 2.6464$, $\triangle P_{0.075}=1.709\rho_d - 3.4391$, and R^2 is 0.8827,
308 0.8199 respectively. The result indicates that $\triangle P_{0.075}$ has a significant correlation with ρ_d. Especially,
309 the greater initial dry density causes the smaller loss of $P_{0.075}$. When IDD is 1.53g/cm^3, P_2 decreases
310 and its change value is -0.16%. When IDD is 1.63~1.81g/cm^3, P_2 increases, and the range of the
311 change are 2.15%~15.45%. The reason for the loss of $P_{0.075}$ and P_2 is that the fine particles are taken
312 away by subsurface runoff. The reason for the increase of P_2 maybe that the particles larger than
313 2mm roll downward, which causes a relative increase in P_2.
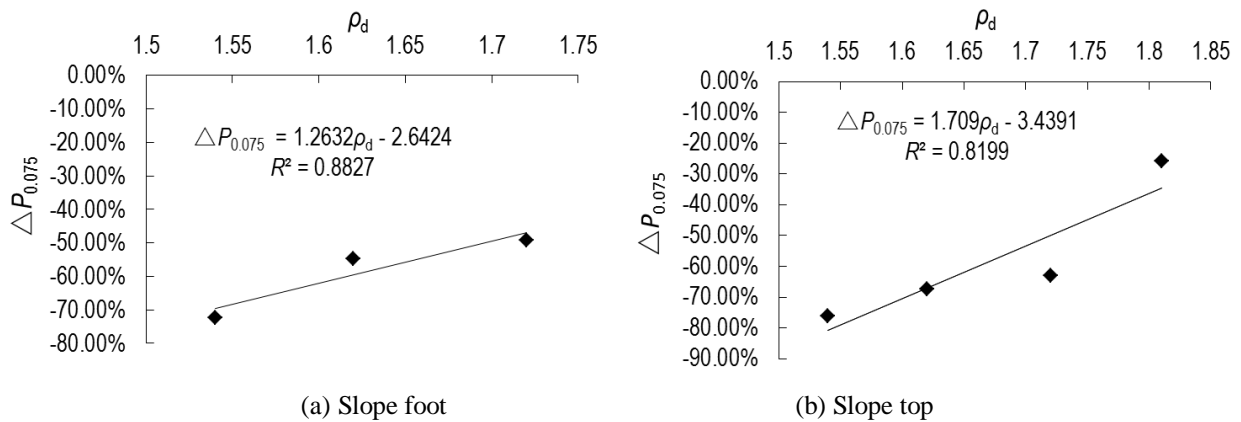
314
315 (a) Slope foot   (b) Slope top
316 **Fig. 12** Relationship between $\triangle P_{0.075}$ and ρ_d

3.4 Critical state of gravel soil

(1) Definition of critical state and calculation of critical void ratio

Under the action of continuous shear load, the state of soil is critical when principal stress q and volume strain ε_v tends to be stable (Casagrande A 1936; Liu et al., 2011; Roscoe et al., 1963; Schofield and Wroth 1968). In the triaxial shear tests, when the axial strain reaches 16%, the deviation stress is stable, and the absolute value of the ratio of $\triangle\varepsilon_v$ to the present ε_v is less than 0.01; at this time, the soil enters the critical state (Liu et al., 2012). The formula (2) indicates that there is a certain relationship between the current void ratio e and ε_v, wherein e_0 is the initial void ratio (Xu et al., 2009). Thus, the critical void ratio e_c also can be calculated by the formula (2).

$$e = (1+e_0)\exp(-\varepsilon_v)-1 \tag{2}$$

(2) The critical state line in the e_c-p' plane

Tab. 4 shows e_c, q and p' for two initial dry densities: 1.94g/cm^3 and 2.00g/cm^3. As shown in Table 4, when the confining pressure is same, two densities have the approximate similar e_c. This result has the consistent principle with existing research (Gabet and Mudd 2006; Iverson et al., 2000). The principle is that the soil with the same granular composition can obtain the approximate critical void ratio in the uniform stress condition (Casagrande A 1936; Roscoe et al., 1963; Schofield and Wroth 1968).

Tab 4. Critical void ratio e_c of gravel soil

Confining pressure σ_3(Kpa)	Initial dry density (g/cm^3)	e_c	q (Kpa)	p' (Kpa)
50	1.94	0.32	93.41	95.98
	2.00	0.34	69.50	84.65
100	1.94	0.30	227.43	213.80
	2.00	0.30	159.14	178.13
150	1.94	0.27	324.79	312.39
	2.00	0.29	181.12	239.86

The fitting curve of e_c and $\ln p'$ is shown in Fig.13(a). The correlation coefficient is 0.8566, which indicates a statistically significant relationship between e_c and p'. According to the normalized residual probability, P-value of 0.964 is greater than the selected significance level, which indicates that the residuals follow a normal distribution. Therefore, the mathematical expression of e_c-$\ln p'$ of gravel soil is as follows:

$$e_c = 0.5241 - 0.04304\ln p' \tag{3}$$

The fitting cure of e_c and $\ln p'$ represents the critical state of soil. It can divide the graphical space into two states. The space above this curve is the contractive zone, and the space below this curve is the dilative zone. If the state parameter (e, p') is determined, the soil state can be judged by this line (Gabet and Mudd 2006; Iverson et al., 2000).

(3) The critical state line in the q-p' plane

The fitting curve of q and the p' is shown in Fig. 13(b). The correlation coefficient is 0.9465, which indicates a statistically significant relationship between q and p'. The mathematical expression of q- p' is as follows:
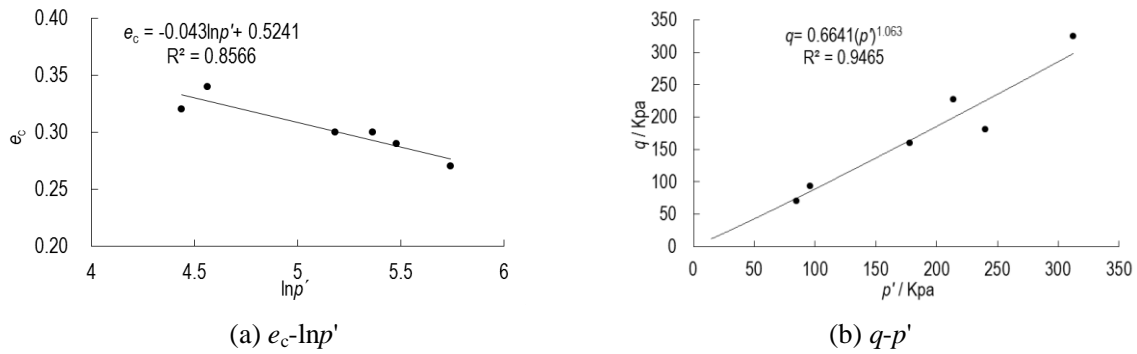
$$q = 0.6641(p')^{1.063} \tag{4}$$

(a) e_c-lnp' (b) q-p'

Fig. 13 Critical sate line of gravel soil

4 Discussion

The relative position of the state parameter (e, p') at the critical state line is shown in Fig.14. The critical states are from Tab.4 and represented by fill dots, and the state parameters of four densities are from Tab.2 and represented by the hollow dots. Fig.14 shows that when IDD is 1.54g/cm^3 and 1.63g/cm^3, contraction occurs at 28cm and 40cm of line 3#. In addition, dilation appears in the remaining positions. These positions include the surface layer of line 3# with the depth of 5~10cm, the depth of 20~33cm of line 2#, the depth of 10~21cm of line 1#. The results show that dilation and contraction are two types of the mechanical state of gravel soil when the landslide initiates. Dilation is the primary type.
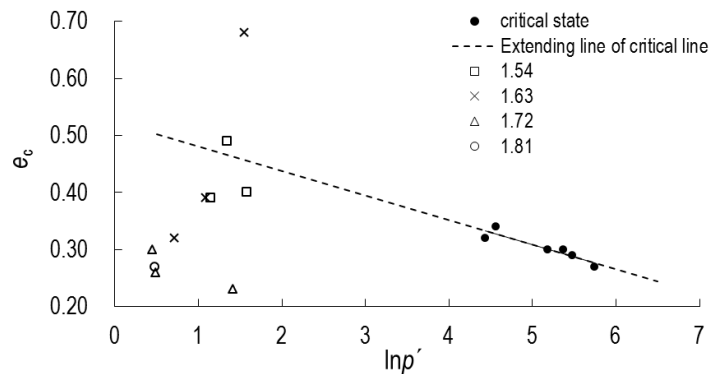
Fig.14 The states of gravel soil

In this research, at the beginning of rainfall, the shallow soil is compacted by seepage force and soil weight. The consequent contraction causes the increase in pore water pressure. However, the process of the rapid rise of PWP is short. After PWP reaches the peak, PWP begins to release. The reason is that the surface soil slowly moves or cracks begin to develop in the slope foot, which causes the sliding force increase. Subsequently, the effective stress decreases and the shearing deformation occurs. At this moment, the loss of shearing strength because of strain softening can be restored. Soil deformation will stop eventually. If there is the sufficient water penetration, pore water pressure can recover, and the soil deformation can continue. It can be seen that the loss and recovery of PMP are the reasons for the dynamic fluctuations of PMP. When soil is dense (relative density $D_r >$ 2/3) and the infiltration rate is less than the rainfall intensity, the soil will not reach the critical state. At this point, the slope can remain stable. The macroscopic phenomenon of soil deformation is mainly local deformation, such as circumferential cracks, partial collapse. If the infiltration rate is greater than the rainfall intensity, the abundant rainfall can break the mechanical balance of slope. However, its process still takes a long time. Therefore, the macroscopic deformation is progressive, such as frequent sliding. When the soil is in a medium dense state ($1/3 < D_r ≤ 2/3$), the loss of the pore

water pressure due to dilation will be recovered, and the shearing deformation will continue. At this moment, the macroscopic deformation will be a sudden failure (Dai et al., 2000; Dai et al., 1999b).

5   Conclusion

(1) The initial dry density can influence the time and mode of landslide occurrence. When IDD is 1.54g/cm^3~1.72g/cm^3, the failure mode of soil changes from progressive sliding to traction sliding. When IDD is less than 1.63g/cm^3, partial sliding is a dominant phenomenon that affects the entire deformation failure. When IDD is 1.72g/cm^3, shear opening and cracks are responsible for deformation failure. Although the total time of overall sliding of loose soil is longer than that of relatively dense soil, the time of partial sliding is shorter.

(2) During the experiments, the first change is VMC of the depth of 10cm, followed by VMC of the depth of 25cm and 40cm. The variation of PWP is inconsistent with the variation of VMC.

(3) The occurrence of landslides is accompanied by change in density and void ratio. The slope foot has the greatest change rate in density. The migration of fine particle and the rearrangement of coarse-fine particle contributed to the reorganization of the microscopic structure, which might be the main reason for the variation of density and void ratio.

(4) The mathematical expression of the critical state line of gravel soil is $e_c=0.5241-0.04304\ln p'$. Mechanical state of gravel soil can be determined by the relative position between the state parameter (e, p') and the critical state line. Dilation and contraction are two types of soil state when the landslide initiates. Dilation is the primary type.

Acknowledgements

This study was funded by the National Natural Science Foundation of China (No 41071058, 41402272, 51609041); Disaster Prevention and Mitigation and Engineering Safety Key Laboratory Project of Guangxi Province (No 2016ZDX09).

References

Been, K.and Jefferies, M.: A state parameter for sands. Geotechnique, 35, 99-112, 1985.

Casagrande A: Characteristics of cohesionless soils affecting the stability of slopes and earth fills. Journal of the Boston Society of Civil Engineers, 23, 13-32, 1936.

Chen, N. S., Cui, P., Wang, X. Y.and Di, B. F.: Testing study on strength reduction of gravelly soil in triggering area of debris flow under earthquake. Chinese Journal of Rock Mechanics and Engineering, 23, 2743-2747, 2004 (in Chinese).

Chen, N. S., Zhou, W., Yang, C. L., Hu, G. S., Gao, Y. C.and Han, D.: The processes and mechanism of failure and debris flow initiation for gravel soil with different clay content. Geomorphology, 121, 222-230, doi: 10.1016/j.geomorph.2010.04.017, 2010.

Chen, N. S., Zhu, Y. H., Huang, Q., Lqbal, J., Deng, M. F.and He, N.: Mechanisms involved in triggering debris flows within a cohesive gravel soil mass on a slope: a case in SW China. Journal of Mountain Science, 14, 611-620, doi: 10.1007/s11629-016-3882-x, 2017.

Chen, Z. Y., Zhou, J. X.and Wang, H. J. (2012) Soil Mechanics. 19th edn. Tsinghua University Press, Beijing

Cui, P., Xiang, L. Z.and Zou, Q.: Risk assessment of highways affected by debris flows in Wenchuan earthquake area. Journal of Mountain Science, 10, 173-189, doi: 10.1007/s11629-013-2575-y, 2013.

Cui, P., Zhuang, J., Qi, , Chen, X. C., Zhang, J., Qiang,and Zhou, X. J.: Characteristics and countermeasures of debris flow in Wenchuan area after the earthquake. Journal of Sichuan University (Engineering Science Edition), 42, 10-19, 2010 (in Chinese).

Dai, F. C., Chen, S. Y.and Li, Z. F.: Analysis of landslide initiative mechanism based on stress-strain behavior of soil.

422   Chinese Journal Of Geotechnical Engineering, 22, 127-130, 2000 (in Chinese).

423   Dai, F. C., Lee, C. F.and Wang, S. J.: Analysis of rainstorm-induced slide-debris flows on natural terrain of Lantau Island,
424   Hong Kong. Engineering Geology, 51, 279-290, doi: S0013-7952(98)00047-7, 1999a.

425   Dai, F. C., Lee, C. F.and Wang, S. J.: Stress-strain behaviour of a loosely compacted voleanic-derived soil and its
426   significance to rainfall-induced fill slope failures. Engineering Geology, 53, 359-370, doi:
427   S0013-7952(99)00016-2, 1999b.

428   Fang, H., Cui, P., Pei, L. Z.and Zhou, X. J.: Model testing on rainfall-induced landslide of loose soil in Wenchuan
429   earthquake region. Natural Hazards and Earth System Science, 12, 527-533, doi: 10.5194/nhess-12-527-2012,
430   2012.

431   Fleming, R. W., Ellen, S. D.and Algus, M. A.: Transformation of dilative and contractive landslide debris into debris
432   flows-An example from marin County, California. Engineering Geology, 27, 201-223, 1989.

433   Gabet, E. J.and Mudd, S. M.: The mobilization of debris flows from shallow landslides. Geomorphology, 74, 207-218,
434   doi: 10.1016/j.geomorph.2005.08.013, 2006.

435   Gao, B., Zhou, J.and Zhang, J.: Macro-meso analysis of water-soil interaction mechanism of debris flow starting process.
436   Chinese Journal of Rock Mechanics and Engineering, 30, 2567-2573, 2011 (in Chinese).

437   Guo, Q. Q. (1998) Engineering features and utilization of coarse-grained soil. 1st edn. The Yellow River Water
438   Conservancy Press, Zhengzhou

439   Igwe, O.: The compressibility and shear characteristics of soils associated with landslides in geologically different
440   localities—case examples from Nigeria. Arabian Journal of Geosciences, 8, 6075-6084, doi:
441   10.1007/s12517-014-1616-3, 2014.

442   Iverson, N. R., Mann, J. E.and Iverson, R. M.: Effects of soil aggregates on debris-flow mobilization: Results from
443   ring-shear experiments. Engineering Geology, 114, 84-92, doi: 10.1016/j.enggeo.2010.04.006, 2010.

444   Iverson, R. M., Reid, M. E., Iverson, N. R., LaHusen, R. G.and Logan, M.: Acute sensitivity of landslide rates to initial
445   soil porosity. Science, 290, 513-516, doi: 10.1126/science.290.5491.513, 2000.

446   Iverson, R. M., Reid, M. E.and Lahusen, R. G.: Debris-flow mobilization from landslides. Annual Review of Earth &
447   Planetary Sciences, 25, 85-138, 1997.

448   Jiang, Z. M., Wang, W., Feng, S. R.and Zhong, H. Y.: Experimental of study on the relevance between stress state and
449   seepage failure of sandy-gravel soil. Shuili Xuebao, 44, 1498-1505, 2013 (in Chinese).

450   Li, Y., Liu, J. J., Su, F. H., Xie, J.and Wang, B. L.: Relationship between grain composition and debris flow
451   characteristics: a case study of the Jiangjia Gully in China. Landslides, 12, 19-28, doi:
452   10.1007/s10346-014-0475-z, 2014.

453   Liang, H., He, S. m., Lei, X. q., Bi, Y. z., Liu, W.and Ouyang, C. j.: Dynamic process simulation of construction solid
454   waste (CSW) landfill landslide based on SPH considering dilatancy effects. Bulletin of Engineering Geology
455   and the Environment, 2, 1-15, doi: 10.1007/s10064-017-1129-x, 2017.

456   Liu, E. L., Chen, S. S.and Li, G. Y.: Critical state of rockfill materials and a constitutive model considering grain crushing.
457   Rock and Soil Mechanics, 32, 148-154, 2011 (in Chinese).

458   Liu, E. L., Qin, Y. L., Chen, S. S.and Li, G. Y.: Investigation on critical state of rockfill materials. Shuili Xuebao, 43,
459   505-511, 519, 2012 (in Chinese).

460   McKenna, J. P., Santi, P. M., Amblard, X.and Negri, J.: Effects of soil-engineering properties on the failure mode of
461   shallow landslides. Landslides, 9, 215-228, doi: 10.1007/s10346-011-0295-3, 2011.

462   Qu, Y. P., Tang, C., Wang, J. L., Tang, H. X., Liu, Y., Chen, H. L.and Huang, W.: Debris flow initiation mechanisms in
463   strong earthquake area. Mountain Research, 30, 336-341, 2012(in Chinese).

464   Reynolds, O.: On the dilatancy of media composed of rigid particles in contact, with experimental illustrations.
465   Philosophical Magazine (Series 5), 20, 469-481, 1885.

466   Roscoe, K. H., Schofield, A. N.and Thuraijajah, A.: Yielding of clays in states wetter than critical. Geotechnique, 13,
467   211-240, 1963.

468   Sassa, K.: The mechanism to initiate debris flows as undrained shear of loose sediments. Internationales Symposium
469   Interpraevent, 73-87, 1984.

470   Schofield, A. N.and Wroth, C. P. Critical state soil mechanics. University of Cambridge, 1968.

471   Schulz, W. H., McKenna, J. P., Kibler, J. D.and Biavati, G.: Relations between hydrology and velocity of a continuously
472   moving landslide - evidence of pore-pressure feedback regulating landslide motion? Landslides, 6, 181-190, doi:
473   10.1007/s10346-009-0157-4, 2009.

474   Tang, C., Li, W. L., Ding, J.and Huang, X. C.: Field Investigation and Research on Giant Debris Flow on August 14,
475   2010 in Yingxiu Town, Epicenter of Wenchuan Earthquake. Earthscience- Journal of China University of
476   Geosciences, 36, 172-180, 2011 (in Chinese).

477   Tang, C.and Liang, J. T.: Characteristics of debris flows in Beichuan epicenter of the Wenchuan earthquake triggered by
478   rainstorm on september 24, 2008. Journal of Engineering Geology, 16, 751-758 (in Chinese), doi:
479   10.1016/j.geomorph.2005.08.013, 2008.

480   Xie, H., Zhong, D. L., Jiao, Z.and Zhang, J. S.: Debris flow in Wenchuan quake-hit area in 2008. Mountain Research, 27,
481   501-509, 2009 (in Chinese).

482   Xu, S. H., Zheng, G.and Xu, G. L.: Critical state constitutive model of sand with shear hardening. Chinese Journal of
483   Geotechnical Engineering, 31, 953-958, 2009 (in Chinese).

484   Yin, Y. P., Cheng, Y. L., Liang, J. T.and Wang, W. P.: Heavy-rainfall-induced catastrophic rockslide-debris flow at
485   Sanxicun, Dujiangyan, after the Wenchuan Ms 8.0 earthquake. Landslides, 13, 9-23, doi:
486   10.1007/s10346-015-0554-9, 2016.

487   YU, B., Ma, Y.and Wu, Y. F.: Investigation of serve debris flow hazards in Wenjia gully of Sichuan province after the
488   Wenchuan earthquake. Jouranl of Enigeering Geology, 18, 827-836, 2010 (in Chinese),.

489   Zhang, M., Hu, R. L.and Yin, Y. P.: Study of transform mechanism of landslide-debris flow with ring shear test. Chinese
490   Journal of Rock Mechanics and Engineering, 29, 822-832, 2010 (in Chinese).

491   Zhu, J., Ding, J.and Liang, J. T.: Influences of the Wenchuan Earthquake on sediment supply of debris flows. Journal of
492   Mountain Science, 8, 270-277, doi: 10.1007/s11629-011-2114-7, 2011.

493   Zhuang, J. Q., Cui, P., Hu, K. H.and Chen, X. Q.: Fine particle size moving and its effective on debris flow initiation.
494   Mountain Research, 33, 713-720, 2015 (in Chinese).

495